Research Article Vol. 57, No. 29 / 10 October 2018 / Applied Optics 8733

applied optics

2 W single-frequency, low-noise 509 nm laser via single-pass frequency doubling of an ECDL-seeded Yb fiber amplifier

Jiaping Qian,[1,2] Lei Zhang,[1,3,4] Huawei Jiang,[1] Shuzhen Cui,[1] Jiaqi Zhou,[1] and Yan Feng[1,*]

[1]Shanghai Institute of Optics and Fine Mechanics, Chinese Academy of Sciences, and Shanghai Key Laboratory of Solid State Laser and Application, Shanghai 201800, China
[2]University of the Chinese Academy of Sciences, Beijing 100049, China
[3]PreciLasers Co. Ltd., Shanghai 201800, China
[4]e-mail: zhangl@siom.ac.cn
*Corresponding author: feng@siom.ac.cn

Received 23 July 2018; revised 17 September 2018; accepted 17 September 2018; posted 18 September 2018 (Doc. ID 340535); published 9 October 2018

A single-frequency low-noise green laser at 509 nm is developed for the study of cesium Rydberg atoms. The laser is generated by single-pass second-harmonic generation of a Yb fiber amplifier seeded with an external cavity diode laser (ECDL) at 1018 nm in a periodically poled MgO-doped lithium-niobate crystal. An up to 2.03 W, 509 nm laser is obtained from a 10.04 W incident 1018 nm laser with a conversion efficiency of 20.2%. The linewidth of the 509 nm laser is estimated to be 40 kHz according to the measured linewidth of 20 kHz of the 1018 nm fundamental laser. The relative intensity noise is 0.038% rms integrated from 10 Hz to 10 MHz. © 2018 Optical Society of America

https://doi.org/10.1364/AO.57.008733

1. INTRODUCTION

Watt-level green lasers at 509 nm have many applications in fundamental research. The 509 nm laser is resonant to the hyperfine transitions of $^6P_{3/2}(F' \rightarrow = 5) \rightarrow nD(n = 39 - 55)$ in cesium atoms, which can be used to produce cesium Rydberg atoms [1,2]. Rydberg atoms display exaggerated collision properties and have potential applications in quantum information and precision measurement. A single-frequency low-noise 509 nm laser is essential in these applications because it can manipulate the Rydberg state of cesium atoms through the two-photon process. Meanwhile, the narrow linewidth and low intensity noise characteristics of the 509 nm laser greatly improve the precision of these applications. Besides, green lasers are pump sources for Ti:sapphire lasers. Today, 532 nm lasers are used in most cases due to their availability. Yet 509 nm lasers have been proved to be a better choice since 509 nm is closer to the absorption peak of Ti:sapphire and thus leads to a higher pump efficiency [3].

However, there is no solid-state gain medium that can directly lase at 509 nm, so nonlinear frequency conversion of the near-infrared laser is an indispensable technology. In the continuous wave (CW) regime, a common method is intracavity second-harmonic generation (SHG) in a diode-pumped "bulk" solid-state laser. This approach takes advantage of the high intracavity power and can produce multi-ten-watt at 532 nm with a high conversion efficiency [4]. Unfortunately, the narrow emission band of the solid gain media leads to a restricted operating wavelength range. Fiber lasers can generate high power output with high beam quality [5], and notably they are widely wavelength tunable in the near-infrared regime and can be tuned to 1018 nm specifically for the current application. Nevertheless, the intracavity SHG scheme is not suitable for fiber lasers because of the relatively high resonator loss [6]. One solution to this problem is to employ an external resonant enhancement cavity [7]. In 2017, Li *et al.* demonstrated a maximum power of 1.13 W at 509 nm with a ring cavity frequency doubler in a periodically poled $KTiOPO_4$ crystal and the conversion efficiency is 71.5% [8]. However, a few disadvantages of this method cannot be ignored. The resonant cavity length must be actively stabilized to ensure that the resonance condition is maintained at all times, resulting in a complex structure and high cost. Besides, this scheme may have difficulty in pulsed lasers.

An attractive alternative is external single-pass nonlinear frequency conversion in periodically poled nonlinear crystals, which is simple, compact, and low cost. Periodically poled MgO-doped crystals such as lithium-niobate (MgO:PPLN) are ideal for the single-pass scheme because of the utilization of the largest nonlinear coefficient and the implementation of an arbitrary wavelength output [9]. In 2015, Tawfieq *et al.* realized 1.7 W 509 nm output in a MgO:PPLN crystal via the

single-pass sum frequency scheme by combining the 978 and the 1063 nm tapered diode lasers with a conversion efficiency of 12.1% [3].

In this paper, we report the development of a 2 W single-frequency low-noise laser at 509 nm for the study of cesium Rydberg atoms. The laser is produced by single-pass SHG of a Yb fiber amplifier seeded by an external cavity diode laser (ECDL) at 1018 nm. The linearly polarized Yb-doped fiber amplifier (YDFA) produces a 10.8 W laser at 1018 nm with an optical conversion efficiency of ~21%. A conversion efficiency of 20.2% to 509 nm is achieved with a 25 mm MgO:PPLN crystal. The laser linewidth and relative intensity noise (RIN) of the laser are characterized in detail. To the best of our knowledge, this is the highest reported CW single-frequency 509 nm laser to date.

2. EXPERIMENTAL SETUP

The laser configuration is shown in Fig. 1, and consists of a single-frequency seed source, a Yb-doped fiber amplifier, and a single-pass frequency-doubling setup. The single-frequency seed source is a 1018 nm ECDL [10] with a fiber pigtailed output of 20 mW and a linewidth of 5 kHz. This seed source is coupled to a home-made all-fiber linearly polarized YDFA [11], which can yield a maximum output power of 10.8 W at 1018 nm. The gain fiber is double-clad polarization-maintaining (PM) fiber with a 10-μm-diameter (NA = 0.075) Yb-doped core surrounded by a 125-μm-diameter pure silica inner cladding. The output beam is linearly polarized with a polarization extinction ratio measured to be 18 dB, owing to the all-PM-fiber configuration.

The collimated 1018 nm fiber amplifier output is optically isolated and incident on a crystal perpendicularly. The frequency-doubling crystal is a 25-mm-long MgO:PPLN fabricated by HC Photonics, whose end faces are coated to low reflectivity $R < 0.2\%$ at both 509 nm and 1018 nm. The maximum nonlinear coefficient (d_{33}) is utilized with the quasi-phase matching (QPM) method of $e + e \rightarrow e$. The crystal is housed in a home-made oven and is maintained at the optimum phase-matching temperature of 26.47°C. The temperature control accuracy of the oven is ±0.01°C, so a steady SH output can be obtained. A half-wave plate (HWP) is adopted to ensure that the incident polarization is parallel to the poling direction of the crystal. A dichroic mirror is employed to separate the incident fundamental light and the generated green light, which is highly transmitting at 509 nm ($T = 95\%$) and highly reflective at 1018 nm ($R > 99.9\%$). According to the optimum focusing condition described by Boyd and Kleinman [12], the confocal parameter b is approximately one third of the crystal length L_C, specifically,

$$b \approx L_c/2.84 = 2n_l\pi\omega_0^2/\lambda_l. \quad (1)$$

Here n_l, λ_l, and ω_0 are the refractive index, the wavelength of the fundamental light, and the beam waist radius inside the crystal, respectively. The optimum beam waist radius inside the crystal is calculated to be 25.76 μm. However, to avoid damage of the MgO:PPLN crystal, the waist radius inside the crystal is expanded to 40 μm instead, corresponding to a confocal parameter of 1.36. A lens L1 with a focus length of 60 mm is used to meet this requirement.

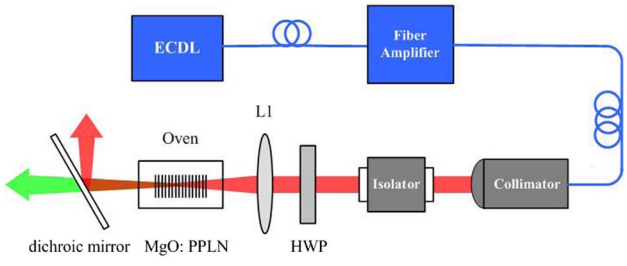

Fig. 1. Schematic diagram of the experimental configuration.

3. RESULTS AND DISCUSSION

The performance of the 1018 nm YDFA is characterized first. The CW single-frequency 1018 nm output power as a function of diode pump power is shown in Fig. 2. When the diode pump power reaches 51.4 W, the output power of the YDFA is 10.8 W, corresponding to an optical–optical conversion efficiency of ~21%. The efficiency is lower than common YDFAs because the length of the gain fiber is chosen to be rather short in order to avoid amplified spontaneous emission (ASE). ASE at 1030–1060 nm is the limiting factor for fiber amplifiers working at the edge of the Yb gain spectrum [13].

The linewidth of the fundamental light is an important factor that affects the conversion efficiency and also determines the linewidth of the frequency-doubled laser. The instantaneous frequency fluctuation power spectral density (PSD) and the linewidth for different integration bandwidths of the YDFA are shown in Fig. 3. This measurement is done by a 120° phase difference interferometer technology based on an unbalanced Michelson interferometer [14]. The frequency fluctuation PSD can fully represent the frequency noise behavior. It can be divided into two regions by the β-separation line as in Fig. 3, since the dominant noise of these two regions has different effects on the laser line shape [15]. In the region in which the frequency fluctuation PSD is above the β-separation line, the noise has an impact on the central part of the line shape and thus on the laser linewidth. Through the frequency fluctuation PSD, the linewidth at different measuring times can be calculated. The green dots in Fig. 3 reveal that the linewidth increases with a decrease of the lower limit of the integration

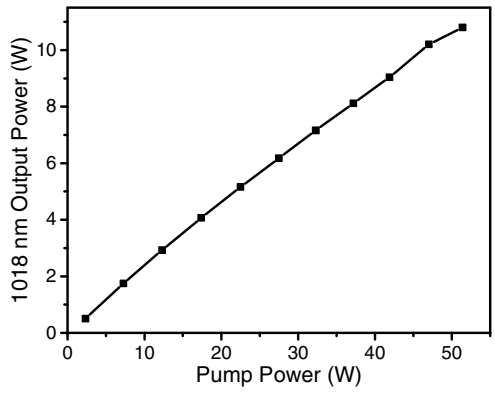

Fig. 2. 1018 nm output power of the YDFA as a function of the pump power.

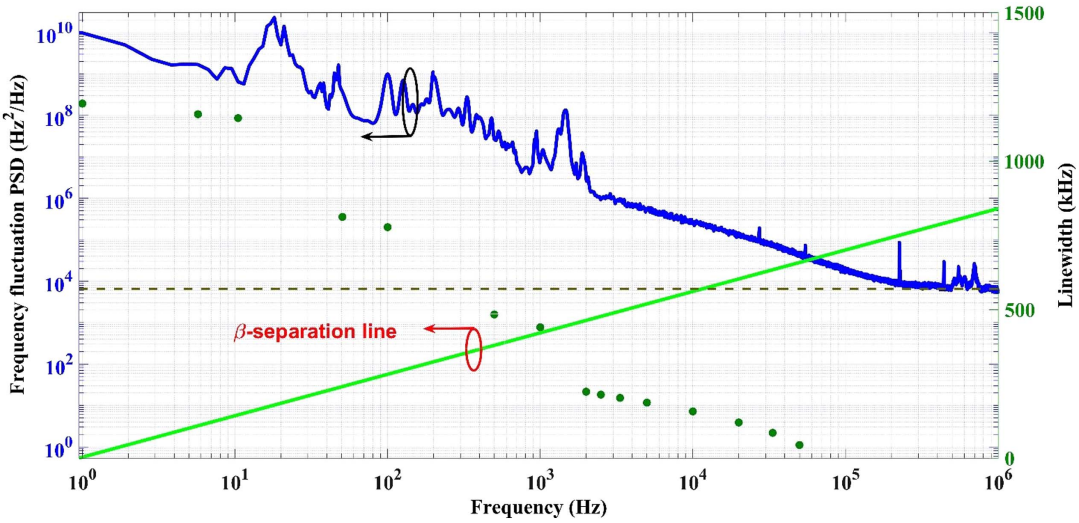

Fig. 3. PSD of instantaneous frequency fluctuation of the YDFA and laser linewidth (FWHM) as a function of frequency.

bandwidth, mainly because of the predominance of flicker noise in this region. In the region in which the frequency fluctuation PSD is below the β-separation line, the noise has a negligible effect on the linewidth, and it contributes only to the wings of the line shape due to white noise accounting for a dominant position. The minimum linewidth of the YDFA can be calculated by πh_0, and h_0 is the frequency fluctuation PSD value at white noise level, which is shown by the brown dotted line in Fig. 3. It can be seen from Fig. 3 that the value of h_0 is about 6200 Hz^2/Hz and that the calculated linewidth of the YDFA is around 20 kHz, from which we estimate the linewidth of the SH output to be 40 kHz.

The fundamental laser is focused into the MgO:PPLN crystal. The temperature of the crystal and the position of the focal lens L1 are fine-tuned for higher SH power. Figure 4 shows the 509 nm power and the conversion efficiency as a function of the incident fundamental power. An up to 2.03 W, 509 nm laser is obtained when the incident fundamental power reaches 10.04 W, corresponding to a conversion efficiency of 20.2%. The actual incident fundamental laser is slightly lower than 10.8 W due to the optical losses accumulated in the isolator, wave plate, and lens. The two numerical fitting curves in Fig. 4

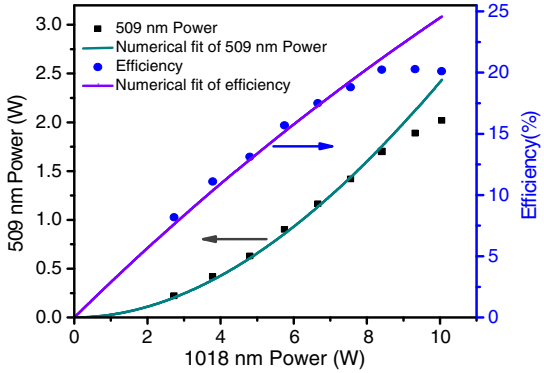

Fig. 4. Dependence of the second-harmonic output power and the conversion efficiency on the incident fundamental power. A numerical fitting is also given.

illustrate the behavior of the SH output when pump depletion is taken into account. Under the plane wave approximation, for single-pass CW frequency doubling, one can establish a set of coupled intensity equations by solving the coupled wave equation in a nonlinear medium. The SH power P_{SHG} can be given by [16]

$$P_{SHG} = P_{laser} \tanh^2\left(\sqrt{\eta_{SHG} P_{laser}}\right). \quad (2)$$

Here P_{laser}, η_{SHG} are the incident fundamental power and the single-pass nonlinear conversion efficiency, respectively. The single-pass nonlinear conversion efficiency is found to be 2.89 %/W by fitting the experimental data. At low fundamental power, the 509 nm power increases nonlinearly as a result of the SHG process, and the theoretical calculation fits well with the experiment data. However, when the fundamental power increases beyond 8 W, both the 509 nm power and the conversion efficiency have a significant drop-off from the theoretical expectations. The data at the high fundamental power level show that the SH output becomes linear with respect to the incident pump power and the conversion efficiency starts to be saturated. These phenomena can be explained by photon absorption [17–19]. On account of the linear and two-photon absorption at both the fundamental and second-harmonic wavelengths, a nonuniform temperature distribution appears in the crystal. Therefore, the phase-matching condition deteriorates, which affects the conversion efficiency of SHG. One can improve the thermal management of the crystal via a better oven design so as to obtain higher power.

The temperature tuning curve of the single-pass SHG is shown in Fig. 5. The Gaussian fitting has a full width at half-maximum (FWHM) bandwidth of $\Delta T = 0.85$°C at the optimum phase-matching temperature of 26.47°C. Through theoretical calculation, the optimum temperature is found to be 29.12°C [20], which is higher than the experimental result. This is primarily because the crystal absorbs a handful of the fundamental and second-harmonic laser and thus accumulates heat inside itself. Moreover, the beam waist radius inside the crystal, the doped concentration, and the angle between the

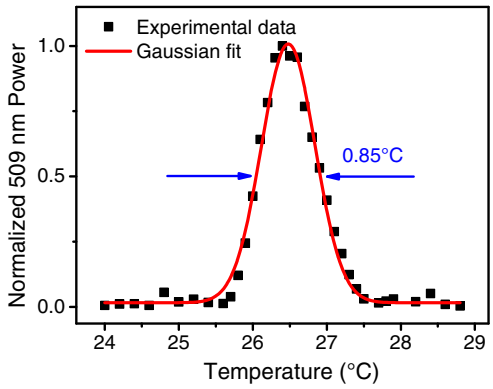

Fig. 5. Measured temperature tuning curve for the MgO:PPLN crystal at 10.04 W incident pump power. A numerical fitting is also given.

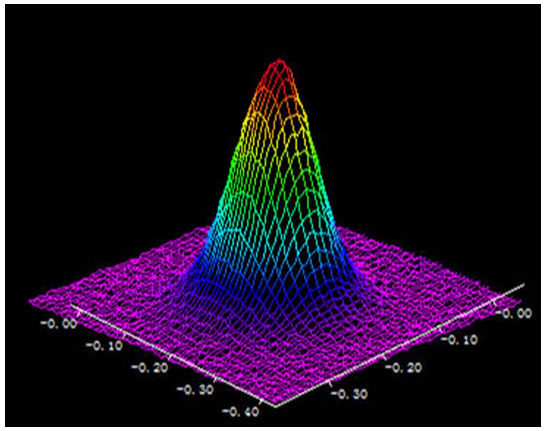

Fig. 7. Far-field beam profile of the 509 nm laser.

poling direction of the crystal and the propagation direction of the incident pump beam will make a difference to the optimum temperature of the crystal.

Laser noise is an important parameter for single-frequency lasers. The RIN of the background, the seed source, and the 509 nm output has been measured and plotted in Fig. 6, respectively. The measurements are completed by two different spectrum analyzers; therefore the RIN before and after 100 kHz has a slight discrepancy. The black curve in Fig. 6 is measured when the photodetector (PD) and the spectrum analyzer are powered on but without any incident beam. Thus the RIN represented by the black curve is composed of the noise introduced by the PD and the spectrum analyzer itself. The RIN of the 509 nm output exhibits a characteristic of $1/f$ type noise in the low-frequency domain. For frequencies

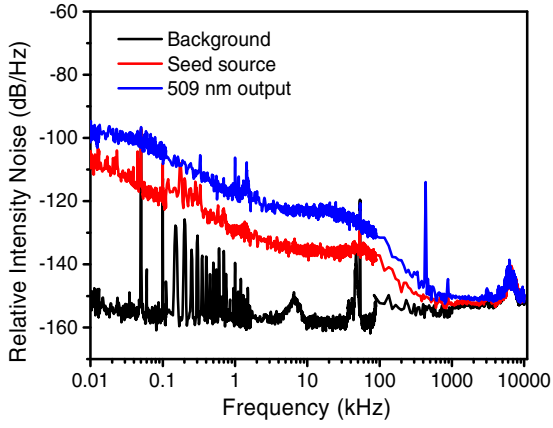

Fig. 6. Relative intensity noise spectral distribution in noise measurements for background, seed source, and the 509 nm output.

<100 kHz, the RIN is less than −94 dB/Hz and the noise is mainly caused by the power fluctuation of the laser diode pump, mechanical vibration, and the fluctuation of the ambient temperature. From 100 kHz to 1 MHz, the RIN decreases from −131 dB/Hz to −150 dB/Hz. In the range of 1 MHz and more, the white noise is dominant and the RIN above 2 MHz is close to the noise background. The rms RIN value can be obtained by the square root of the integrated RIN, and the 509 nm output reveals an ultra-low rms RIN value of only 0.038% in the 10 Hz–10 MHz spectral range. Different applications require a relatively low noise level in a specific spectral range. Table 1 shows the rms RIN value measured in different spectral ranges for the 509 nm output and the seed source. The major part of the noise of the 509 nm output is concentrated in the frequency range of 100 kHz–1 MHz because there is a spike at 433 kHz in the noise spectrum, which comes from the control circuits of the YDFA and might be eliminated by optimizing the circuit parameters.

The beam propagation factors of the SHG have not be measured due to the lack of experimental conditions. But we have reason to believe that the 509 nm output is near-diffraction-limited owing to the single-frequency, single-mode fundamental laser and the single-pass SHG scheme. Figure 7 shows the far-field image of the 509 nm laser, which has a perfect Gaussian intensity distribution.

4. CONCLUSION

We have developed a single-frequency low-noise green laser at 509 nm, and its linewidth and intensity noise characteristics are ideal for the study of cesium Rydberg atoms. It is based on a simple and compact single-pass SHG in a 25 mm MgO:PPLN crystal of an ECDL-seeded Yb fiber amplifier. An up to 2.03 W, 509 nm laser has been achieved with an optical conversion efficiency of 20.2% from 1018 nm. The laser has a

Table 1. Frequency Partition of the Intensity Noise in Both 509 nm Output and Seed Source

Frequency Range	10 Hz–1 kHz	1 kHz–10 kHz	10 kHz–100 kHz	100 kHz–1 MHz	1 MHz–10 MHz
509 nm output [% rms]	0.0116	0.0084	0.0149	0.0267	0.0126
Seed source [% rms]	0.0037	0.0021	0.0048	0.0034	0.0113

Lorentz linewidth of about 40 kHz and an rms RIN value of only 0.038% in 10 Hz–10 MHz spectral range. As far as we know, it is the highest CW single-frequency power at 509 nm. Thermal dephasing is found to reduce the conversion efficiency when the fundamental power is greater than 8 W. The thermal management of the crystal can be improved by better oven design, which can lead to higher 509 nm power. Further power scaling and improvement in the laser performance is possible by developing a higher power 1018 nm fiber laser and nonlinear optical crystals with a higher damage threshold such as periodically poled MgO-doped stoichiometric lithium tantalate (PPMgSLT) [18,21] and periodically poled $LaBGeO_5$ (PPLBGO) [22]. Notably, the laser is also an interesting compact pump source for a Ti:sapphire laser.

Funding. National Natural Science Foundation of China (NSFC) (61575210).

REFERENCES

1. J. He, D. Pei, J. Wang, and J. Wang, "Velocity-selective spectroscopy measurements of Rydberg fine structure states in a hot vapor cell," Chin. Phys. B **26**, 113202 (2017).
2. J. Zhao, X. Zhu, L. Zhang, Z. Feng, C. Li, and S. Jia, "High sensitivity spectroscopy of cesium Rydberg atoms using electromagnetically induced transparency," Opt. Express **17**, 15821–15826 (2009).
3. M. Tawfieq, O. B. Jensen, A. K. Hansen, B. Sumpf, K. Paschke, and P. E. Andersen, "Efficient generation of 509 nm light by sum-frequency mixing between two tapered diode lasers," Opt. Commun. **339**, 137–140 (2015).
4. L. McDonagh and R. Wallenstein, "Low-noise 62 W CW intracavity-doubled TEM_{00} Nd:YVO_4 green laser pumped at 888 nm," Opt. Lett. **32**, 802–804 (2007).
5. D. J. Richardson, J. Nilsson, and W. A. Clarkson, "High power fiber lasers: current status and future perspectives [invited]," J. Opt. Soc. Am. B **27**, B63–B92 (2010).
6. V. A. Akulov, D. M. Afanasiev, S. A. Babin, D. V. Churkin, S. I. Kablukov, M. A. Rybakov, and A. A. Vlasov, "Frequency tuning and doubling in Yb-doped fiber lasers," Laser Phys. **17**, 124–129 (2007).
7. T. Südmeyer, Y. Imai, H. Masuda, N. Eguchi, M. Saito, and S. Kubota, "Efficient 2nd and 4th harmonic generation of a single-frequency, continuous-wave fiber amplifier," Opt. Express **16**, 1546–1551 (2008).
8. G. Li, S. Li, X. Wang, P. Zhang, and T. Zhang, "High efficient generation of over 1 W 509 nm laser beam by a ring cavity frequency doubler with periodically poled $KTiOPO_4$," Appl. Opt. **56**, 55–60 (2017).
9. K. Mizuuchi, K. Yamamoto, and M. Kato, "Harmonic blue light generation in X-cut MgO:$LiNbO_3$ waveguide," Electron. Lett. **33**, 806–807 (1997).
10. C. J. Hawthorn, K. P. Weber, and R. E. Scholten, "Littrow configuration tunable external cavity diode laser with fixed direction output beam," Rev. Sci. Instrum. **72**, 4477–4479 (2001).
11. J. Hu, L. Zhang, H. Liu, K. Liu, Z. Xu, and Y. Feng, "High power room temperature 1014.8 nm Yb fiber amplifier and frequency quadrupling to 253.7 nm for laser cooling of mercury atoms," Opt. Express **21**, 30958–30963 (2013).
12. G. D. Boyd and D. A. Kleinman, "Parametric interaction of focused Gaussian light beams," J. Appl. Phys. **39**, 3597–3639 (1968).
13. J. Hu, L. Zhang, and Y. Feng, "Widely tunable single-mode Yb-doped all-fiber master oscillator power amplifier," IEEE Photon. Technol. Lett. **27**, 2559–2562 (2015).
14. D. Xu, F. Yang, D. Chen, F. Wei, H. Cai, Z. Fang, and R. Qu, "Laser phase and frequency noise measurement by Michelson interferometer composed of a 3×3 optical fiber coupler," Opt. Express **23**, 22386–22393 (2015).
15. G. Di Domenico, S. Schilt, and P. Thomann, "Simple approach to the relation between laser frequency noise and laser line shape," Appl. Opt. **49**, 4801–4807 (2010).
16. O. B. Jensen, P. E. Andersen, B. Sumpf, K.-H. Hasler, G. Erbert, and P. M. Petersen, "1.5 W green light generation by single-pass second harmonic generation of a single-frequency tapered diode laser," Opt. Express **17**, 6532–6539 (2009).
17. Z. M. Liao, S. A. Payne, J. Dawson, A. Drobshoff, C. Ebbers, D. Pennington, and L. Taylor, "Thermally induced dephasing in periodically poled KTP frequency-doubling crystals," J. Opt. Soc. Am. B **21**, 2191–2196 (2004).
18. O. A. Louchev, N. E. Yu, S. Kurimura, and K. Kitamura, "Thermal inhibition of high-power second-harmonic generation in periodically poled $LiNbO_3$ and $LiTaO_3$ crystals," Appl. Phys. Lett. **87**, 131101 (2005).
19. S. V. Tovstonog, S. Kurimura, I. Suzuki, K. Takeno, S. Moriwaki, N. Ohmae, N. Mio, and T. Katagai, "Thermal effects in high-power CW second harmonic generation in Mg-doped stoichiometric lithium tantalate," Opt. Express **16**, 11294–11299 (2008).
20. A. Bruner, D. Eger, M. B. Oron, P. Blau, M. Katz, and S. Ruschin, "Temperature-dependent Sellmeier equation for the refractive index of stoichiometric lithium tantalate," Opt. Lett. **28**, 194–196 (2003).
21. S. Chaitanya Kumar, G. K. Samanta, and M. Ebrahim-Zadeh, "High-power, single-frequency, continuous-wave second-harmonic-generation of ytterbium fiber laser in PPKTP and MgO:sPPLT," Opt. Express **17**, 13711–13726 (2009).
22. J. Hirohashi, T. Taniuchi, K. Imai, and Y. Furukawa, "Non-walk-off second harmonic 532 nm generation by PP-LBGO at room temperature operation," in *Advanced Solid State Lasers*, OSA Technical Digest (online) (Optical Society of America, 2015), paper AM2A.6.